Research Article

Maha Abdallah Alnuwaiser and Mohamed Rabia*

A promising photocathode for green hydrogen generation from sanitation water without external sacrificing agent: silver-silver oxide/poly (1*H*-pyrrole) dendritic nanocomposite seeded on poly-1*H* pyrrole film

https://doi.org/10.1515/phys-2024-0103
received August 17, 2024; accepted November 14, 2024

Abstract: A novel photocathode has shown promise for generating green hydrogen from sanitation water at a rate of 50 µmol/h per 10 cm², using waste water as an electrolyte in a three-electrode cell. This photocathode is composed of two layers: a poly(1*H*-pyrrole) seeding layer topped with a silver-silver oxide/poly(1*H*-pyrrole) (Ag-Ag_2O-P1HP) dendritic nanocomposite. The nanocomposite exhibits broad light absorption up to 660 nm and possesses a bandgap of 1.8 eV. SEM images reveal that the Ag-Ag_2O-P1HP nanocomposite consists of well-ordered semi-spherical nanoparticles, with an average size between 80 and 100 nm. These spherical nanoparticles offer a large surface area, which enhances photon absorption and trapping efficiency. Additionally, the crystalline structure is characterized by a small crystal size of 32 nm, further contributing to the material's efficiency. Hydrogen generation performance was evaluated by measuring the current density (J_{ph}) under white light and monochromatic light, compared to the dark current (J_o). The photocathode's sensitivity was tested using four different monochromatic wavelengths: 540, 440, 340, and 730 nm. The first three wavelengths – 540, 440, and 340 nm – resulted in high J_{ph} values of −0.19, −0.20, and −0.21 mA/cm², respectively, indicating significant hydrogen production. Conversely, the 730 nm wavelength produced a lower J_{ph} value of −0.17 mA/cm², as the energy at this wavelength is insufficient to induce significant bond vibrations, resulting in limited hydrogen production. The high efficiency, combined with the straightforward fabrication of this photocathode, suggests that it could be scaled up as a prototype for industrial hydrogen generation applications.

Keywords: green hydrogen generation, sanitation water, poly(1*H*-pyrrole), silver-silver oxide, plasmonic material

Nomenclature

F	Faraday constant
FTIR	Fourier transform infrared spectroscopy
J_o	current density in the dark
J_{ph}	current density in light
P1HP	poly(1*H*-pyrrole)
SEM	scanning electron microscope
TEM	transmission electron microscope

Greek symbols

D	crystalline size
λ	light wavelength
ß	full-width half maximum

1 Introduction

Hydrogen is an eco-friendly energy source that offers a solution to both green chemistry development beside the energy crisis. The photocatalytic water-splitting process for hydrogen production has gained significant attention as an

* **Corresponding author: Mohamed Rabia,** Nanomaterials Science Research Laboratory, Chemistry Department, Faculty of Science, Beni-Suef University, Beni-Suef, 62514, Egypt,
e-mail: mohamedchem@science.bsu.edu.eg
Maha Abdallah Alnuwaiser: Department of Chemistry, College of Science, Princess Nourah bint Abdulrahman University, P.O. Box 84428, Riyadh, 11671, Saudi Arabia, e-mail: maalnoussier@pnu.edu.sa

abundant element H_2 fuel is used in transportation, power generation, and industrial processes [1,2]. Hydrogen energy is crucial due to its capacity to produce power without releasing harmful emissions. When used as a fuel, hydrogen's sole by-product is water, making it an environmentally sustainable and clean energy source. Unlike fossil fuels, hydrogen does not lead to greenhouse gas emissions, air pollution, or the formation of harmful particulate matter, positioning it as a promising alternative for reducing environmental impact [3].

In 2021, 94 million tons is consumed from H_2 fuel marking a notable 5% increase from the previous year. This growth was particularly evident in traditional hydrogen applications, especially in chemical processes, and represented a significant recovery from the impacts of the COVID-19 pandemic. According to the IEA agency, USA, hydrogen demand is projected to escalate to 115 million tons by 2030. Hydrogen's potential extends well beyond energy production, offering substantial advantages over conventional fossil fuels. As a clean fuel, it plays a crucial role in green chemistry by promoting a more environmentally friendly approach and minimizing or even eliminating the production of harmful particulate matter [4,5]. This positions hydrogen as a significant contributor to tackling global environmental issues. Furthermore, its versatility as an energy carrier allows it to be used in a wide range of applications, including powering vehicles, generating electricity, and supporting various industrial processes [6–8].

The growing interest in hydrogen is also driven by its potential to enhance energy security. A variety of sources can be used for producing hydrogen gas, including organic materials, biomass, and water, making it a flexible option for different regions and energy systems. This diversity in production methods contributes to a more resilient and secure energy supply [4]. Furthermore, the advancements in hydrogen production technologies, such as photocatalytic water splitting, are making hydrogen a more viable and cost-effective energy solution. These technologies are continually being developed and optimized, enhancing their efficiency and reducing their costs. As a result, hydrogen is becoming an increasingly attractive option for a variety of applications, from small-scale residential energy systems to large-scale industrial operations [9,10].

Water splitting relies on the use of photocatalytic materials, such as metal oxides, which are highly effective for producing green hydrogen. To increase their efficiency, the morphology of these materials is often optimized, *e.g.*, by creating a porous structure or scaling them down to the nanoscale. The combination of photocatalysts with plasmonic materials can significantly improve their light absorption properties. This enhancement occurs because plasmonic materials, when used as coatings, amplify light capture and generate hot electrons that facilitate the water-splitting reaction. Silver (Ag) stands out as an excellent plasmonic material due to its superior performance, affordability, and resistance to corrosion, making it a valuable addition to photocatalytic systems. The synergy between silver and photocatalytic materials boosts the overall effectiveness of the process, providing a promising approach to advancing hydrogen production technologies [11,12].

One approach to modifying metal oxides is by creating composites with polymer semiconductors. These modifications are designed to boost the photocatalytic efficiency and stability of the materials, making them more effective for hydrogen production and expanding their potential uses in other applications. By combining metal oxides with polymer semiconductors, researchers aim to improve the overall performance of these materials, allowing for more efficient energy conversion and increased durability. This enhancement not only makes them more suitable for practical hydrogen production but also opens up new possibilities for their use in various other fields where enhanced photocatalytic properties are required [13,14].

A well-known triad of conducting polymers includes polythiophene, polyaniline, and P1HP. Among these, P1HP is particularly attractive for a variety of applications. P1HP is used in various fields, such as outer-coating layers. The form and usage of P1HP can be extensively tailored based on its properties including the nanoscale particle size combined with the photocatalytic behavior. P1HP's coating ability makes it an ideal material for modifying and enhancing absorbance and opens up significant opportunities for light-based energy applications [15,16].

Previous studies have typically focused on estimating hydrogen gas generation using complex techniques, often relying on fresh water as an electrolyte or incorporating acidic or basic sacrificing agents. These factors present challenges to the efficiency and effectiveness of hydrogen gas production [17].

Herein, this study introduces a novel photocathode, Ag-Ag_2O-P1HP/P1HP, which shows great potential for producing green hydrogen from sanitation water without the need for any external sacrificing agents. The chemical composition of this nanocomposite was thoroughly analyzed using various techniques such as X-ray diffraction (XRD), X-ray photoelectron spectroscopy (XPS), and Fourier transform infrared spectroscopy (FTIR), alongside additional electrical, optical, and morphological assessments. The photocathode's sensitivity was rigorously tested under four monochromatic wavelengths: 540, 440, 340, and 730 nm, and further evaluated by comparing its performance in both light illuminations and darkness. The hydrogen gas rate is determined, and the sensitivity was assessed by examining the

differences between the J_{ph} and J_o values. A comparative analysis with other studies in the literature highlighted the advantages of this photocathode, particularly in terms of cost-effectiveness and technical performance, including the generated current density. The combination of high efficiency and the straightforward fabrication process indicates that this photocathode is a promising candidate for scaling up as a prototype for industrial hydrogen generation applications.

2 Materials and methods

2.1 Materials

Silver nitrate ($AgNO_3$ 99.9%, Pio-Chem co, Egypt), HCl (36%, Merck, Germany), acetic acid (CH_3COOH, 99.9%, Pio-Chem co, Egypt), Pyrrole (Across Co., 99.9%, USA), ethanol (C_2H_5OH, 99.9%, Merck, Germany), and $(NH_4)_2S_2O_8$ (99.9%, Pio-Chem co, Egypt)

2.2 Fabrication of Ag-Ag_2O-P1HP/P1HP photocathode using photopolymerization reaction

The synthesis of the P1HP material as a promising seeding layer begins with the preparation of a clean glass substrate. To create this seeding layer, pyrrole is dissolved in 0.5 M HCl while being stirred thoroughly. For the oxidant preparation, $(NH_4)_2S_2O_8$ is dissolved in 50 ml of water. To complete the synthesis, the oxidant is quickly added to the pyrrole solution, leading to full polymerization and the formation of a P1HP thin film.

The preparation of the Ag-Ag_2O-P1HP/P1HP photocathode involves a reaction similar to the previous oxidation of pyrrole to P1HP. In this case, however, $AgNO_3$ serves as the oxidant, with a pyrrole to oxidant ratio of 1:2.5. Here pyrrole is dissolved in acetic acid. During the addition of the oxidant to the pyrrole solution, a vacuum metal halide lamp is used to illuminate the solution, facilitating the photopolymerization reaction.

The reaction results in the formation of an Ag-Ag_2O-P1HP/P1HP photocathode thin film. This film undergoes further treatment, including immersion in distilled water and subsequent drying at 60°C. Once these steps are completed, the electrode is ready for characterization and electrochemical testing for green hydrogen generation. Figure 1 depicts the preparation procedure of this promising photocathode.

2.3 Ag-Ag_2O-P1HP/P1HP photocathode for hydrogen generation photoelectrochemically

Green hydrogen generation is achieved photoelectrochemically using a specially fabricated Ag-Ag_2O-P1HP/P1HP photocathode. This process utilizes a three-electrode cell setup, with sanitation water as the primary electrolyte. Sanitation water is chosen for its potential to be converted into green hydrogen gas, contributing to renewable energy goals. Within this setup, the photocathode (main working electrode), where all reduction reactions take place, results in the production of green hydrogen gas. The efficiency of the photocathode is assessed by measuring the J_{ph} produced under light illumination, as this reflects the electrode's capability to generate hydrogen gas.

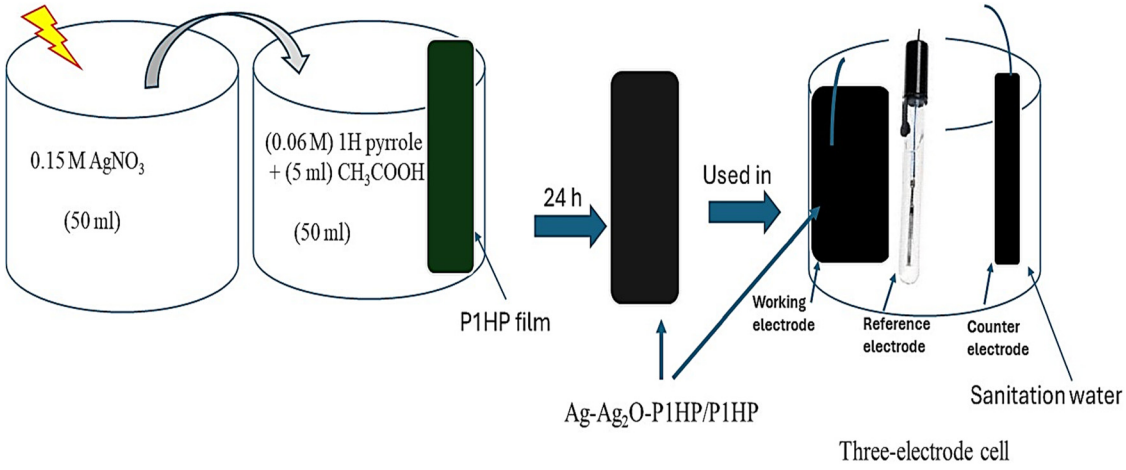

Figure 1: The schematic steps for the synthesizing of Ag-Ag_2O-P1HP/P1HP photocathode and their position inside the three-electrode cell for H_2 gas generation.

The potential of the photocathode is determined relative to a calomel reference electrode. To quantify the cell's efficiency, the produced moles of hydrogen are calculated using the Faraday equation (Eq. (1)), which involves the Faraday constant (F) and the change in time (dt) [17]. The light source for the experiment is a vacuum metal halide lamp, capable of providing complete white light illumination. Electrochemical measurements are carried out using a CHI608E device through linear sweep voltammetry, and the relationship between current and time is analyzed *via* a chopped relation.

Furthermore, the sensitivity of the photocathode to different wavelengths is examined by measuring J_{ph} under various wavelengths. This approach helps determine how the photoelectrode responds to different light conditions. This comprehensive method allows for the evaluation of the photocathode's efficiency and its potential application in generating green hydrogen from contaminated water, making significant strides toward sustainable and renewable energy solutions.

The incident photon-to-current efficiency (IPCE) for hydrogen gas production represents the conversion of photons into current. This calculation can be estimated based on the photon intensity (P) and different wavelengths (λ), using Eq. (2) [18,19], while taking the J_{ph} into account. Meanwhile, the estimation of solar-to-hydrogen conversion efficiency (STH) is evaluated using Eq. (3) [20] (Table 1).

$$H_2\text{mole} = \int_0^t J_{ph} \cdot dt/F, \tag{1}$$

$$\text{IPCE} = 1{,}240 \cdot \frac{J_{ph}}{P \cdot \lambda} \cdot 100, \tag{2}$$

$$\text{STH} = 1.23 \cdot \frac{J_{ph}}{P} \cdot 100. \tag{3}$$

Table 1: Sanitation water with their conc. relative to metals and other materials [17,21]

Material or element	Conc. (µg/L)
Ba^{3+}	0.002
F^-	0.001
Phenols	0.015
Hg^{2+}	0.005
Ni^{3+}	0.01
Cr^{3+}	0.001
Mn^{2+}	0.001
As^{3+}	0.05
Co^{2+}	0.002
Al^{3+}	0.003
Cd^{3+}	0.05
NH_3	0.005
Cu^{2+}	0.00015
Pb^{2+}	0.05
Fe^{3+}	0.0015
Ag^+	0.02
Zn^{2+}	0.005
CN^{-1}	0.01
Coli groups	0.004/0.1 cm^3
Other cations	0.01
Industrial washing	0.05
Pesticides	0.02

3 Results and discussion

3.1 Ag-Ag_2O-P1HP/P1HP nanocomposite physio-chemical characterization

The functional group analysis of the Ag-Ag_2O-P1HP nanocomposite involves key steps to highlight the composite's structure. The FTIR spectrum, depicted in Figure 2(a), identifies the primary functional groups at wavenumbers 1,631, 1,399, 1,036, and 937 cm^{-1}, indicating the presence of the P1HP ring structure. The incorporation of Ag-Ag_2O significantly influences the vibrational characteristics of the composite, as indicated by the distinct enhancement of the band at 617 cm^{-1}. In the original pristine P1HP polymer, this band, attributed to the C–H out-of-plane bending vibrations, is present but appears weak due to the free rotation of bonds in the P1HP structure, which affects the intensity of certain vibrational modes. However, upon integrating Ag-Ag_2O into the composite, the 617 cm^{-1} band becomes noticeably stronger. This change suggests that the presence of Ag-Ag_2O alters the local molecular environment, thereby impacting the organic C–H vibrations. The interaction between the Ag-Ag_2O and the polymer matrix appears to enhance the rigidity or restrict the rotational freedom within the polymer, leading to a more pronounced vibrational mode. Consequently, the strengthening of the band at 617 cm^{-1} reflects the impact of Ag-Ag_2O on the polymer's structural dynamics, particularly its influence on the vibrational behavior of the C–H bonds within the composite. The detailed functions of these groups are summarized in Table 2.

The crystallinity behavior and chemical structure of the Ag-Ag_2O-P1HP nanocomposite are analyzed using XRD (Figure 2(b)). The peaks corresponding to Ag and Ag_2O materials are prominently observed. The peak at 37.9° corresponds to the (200) growth direction of Ag_2O (JCPDS No. 76-1393), while the peaks at 44.0°, 64.1°, and 77.3° correspond to the (200), (220), and (331) growth directions of

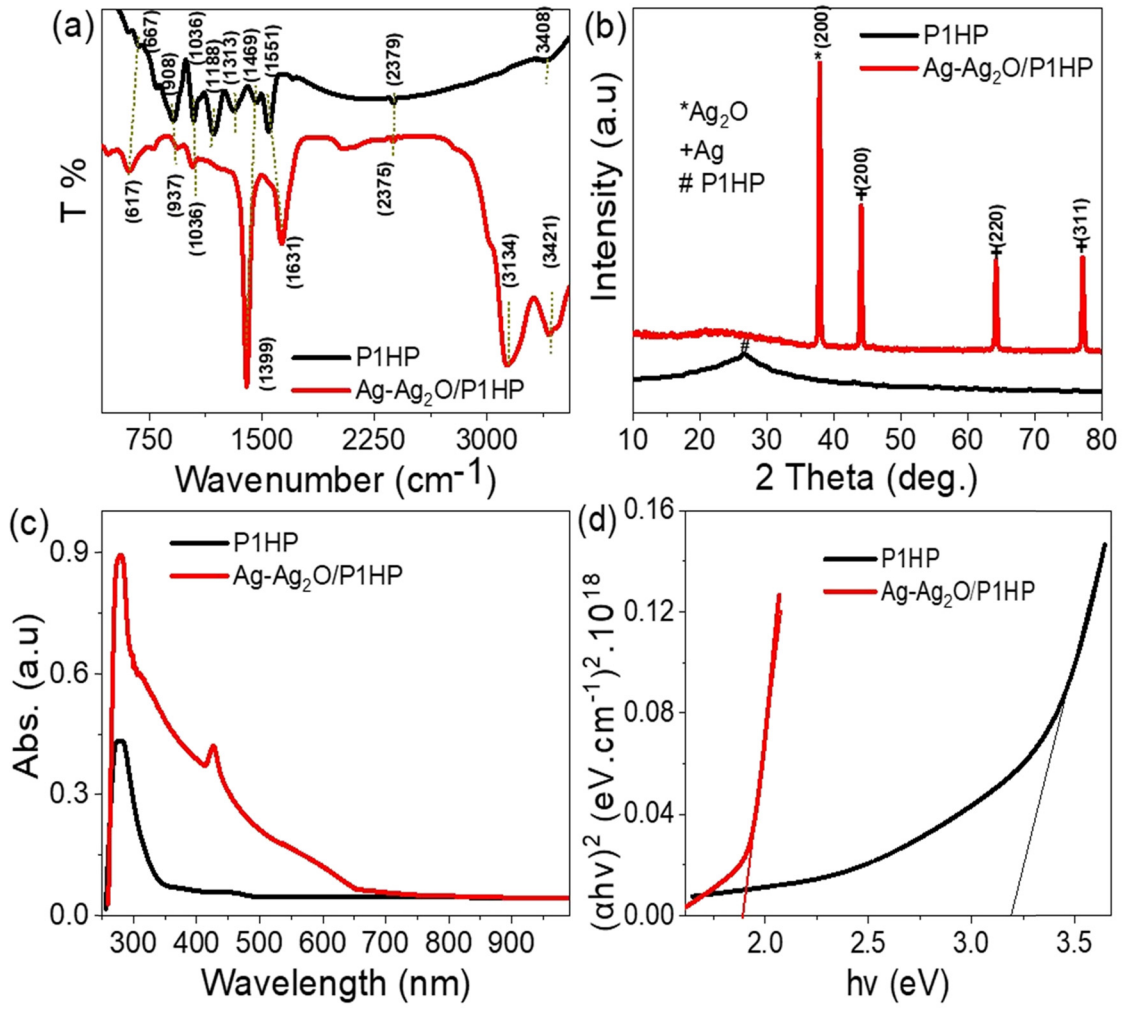

Figure 2: Chemical analysis of the Ag-Ag_2O-P1HP nanocomposite: (a) FTIR spectroscopy and (b) XRD pattern. Optical analysis of the nanocomposite: (c) absorbance and (d) bandgap.

Table 2: Estimated FTIR analyses reflect the Ag-Ag_2O-P1HP nanocomposite structure

Group and its value (cm^{-1})		Functional group
Ag-Ag_2O-P1HP	**P1HP**	
3,421	3,408	N–H [22]
1,631, 1,399, 1,036, and 937	1,551, 1,469, 1,313, 1,188, 1,036, and 908	P1HP ring [23]
617	—	Ag-O

Ag, respectively, (JCPDS file No. 87-0720) [24]. The P1HP component remains amorphous in both its composite form with Ag materials and in its pristine state. The significant improvements within the composite are attributed to the presence of inorganic materials Ag and Ag_2O, which enhance the overall nanocomposite structure.

The crystalline size is calculated using the Scherrer equation (Eq. (4)) [25,26], which depends on the incident angle 2θ and the peak width at half maximum. Applying the 2θ value of 37.9° in the Scherrer equation, the estimated crystalline size is determined to be 32 nm.

$$D = \frac{0.94\lambda}{ß\cos\theta}. \quad (4)$$

The sensitivity of the fabricated Ag-Ag_2O-P1HP nanocomposite to incident photons is assessed through optical analyses, as shown in Figure 2(c). The optical absorbance of the nanocomposite shows a significant enhancement compared to pristine P1HP. This improvement is reflected in the higher optical absorbance value and the broad absorption range extending up to 660 nm. This indicates the composite's capability to promote electron transfer to a higher energy level (conduction band) under light illumination,

resulting in a substantial accumulation of electron clouds in the conduction band due to photon exposure [27,28].

Given this impressive optical behavior, the bandgap is evaluated as illustrated in Figure 2(d). There is a notable difference in bandgap values between the composite and P1HP. The estimated bandgap values are 1.8 eV for the nanocomposite and 3.2 eV for the pristine P1HP. The smaller bandgap of the composite enhances its ability to absorb photons in the UV and visible regions, thereby generating a significant number of hot electrons on the composite's surface. Overall, the optical analyses reveal that the Ag-Ag_2O-P1HP nanocomposite exhibits superior photon absorbance and electron transfer capabilities compared to pristine P1HP. The enhanced optical absorbance and broad absorption spectrum suggest that the composite is highly efficient in capturing and utilizing light energy. The reduced bandgap of the composite further supports its effectiveness in absorbing UV and visible light, leading to the generation of hot electrons that can be harnessed for various applications. This makes the Ag-Ag_2O-P1HP nanocomposite a promising material for optical and photoelectrochemical applications.

The oxidation states with the elemental types of the synthesized Ag-Ag_2O-P1HP nanocomposite are estimated using XPS, as illustrated in Figure 3. The survey spectrum (Figure 3(a)) identifies all elements present in the composite, showing nitrogen (N) and carbon (C) from P1HP associated with the 1s orbital at binding energies of 400 eV and 285.3 eV, respectively. Oxygen (O), representing the oxide source, is observed at 532 eV, corresponding to the 1s orbital.

To further clarify the presence of the Ag element in both its metallic and oxide forms, Figure 3(b) highlights the detailed spectra. The doublet peaks for the Ag element reveal contributions from both Ag_2O and metallic Ag in the composite. The binding energies for the $Ag3d_{5/2}$ and $Ag3d_{3/2}$ orbitals of Ag^+ are observed at 367.8 and 373.6 eV, correspondingly. For the metallic Ag, these orbitals appear at 368.6 and 374.2 eV, respectively [29].

These XPS data support the XRD findings, confirming the presence of both Ag_2O and Ag materials within the P1HP matrix, thereby forming the Ag-Ag_2O-P1HP nanocomposite. This comprehensive analysis emphasizes the incorporation of these elements and their respective oxidation states, highlighting the composite's complex structure.

The morphological behavior significantly impacts the optical properties and applications of the synthesized Ag-Ag_2O-P1HP nanocomposite. This composite's morphology is analyzed using various analytical tools such as SEM, TEM, and theoretical estimation, as illustrated in Figure 4.

Figure 4(a) shows the SEM image of the Ag-Ag_2O-P1HP nanocomposite, revealing well-ordered semi-spherical nanoparticles with an average size ranging from 80 to 100 nm. The spherical shape of these nanoparticles provides a large surface area for photon absorption, making the composite highly efficient in photon trapping and capturing. Figure 4(c) displays the TEM image, which further confirms this behavior. The image shows that the Ag-Ag_2O material is embedded within the P1HP matrix, with variations in structure indicated by different colors (dark and gray) representing the distinct materials. The estimated size of the composite from the TEM

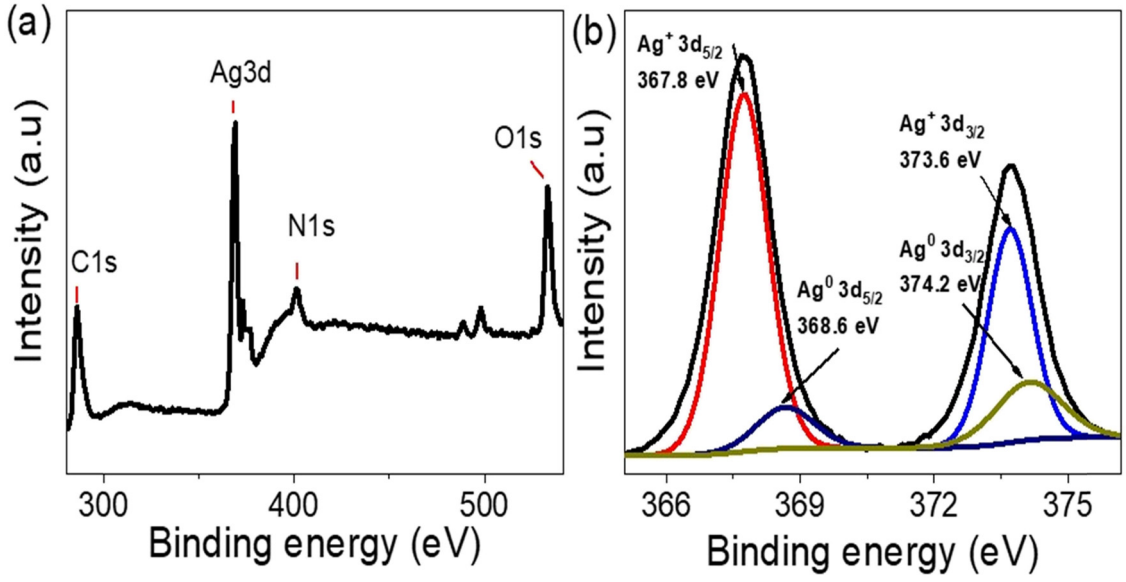

Figure 3: The Ag-Ag_2O-P1HP nanocomposite XPS chemical characterization: (a) survey and (b) Ag element.

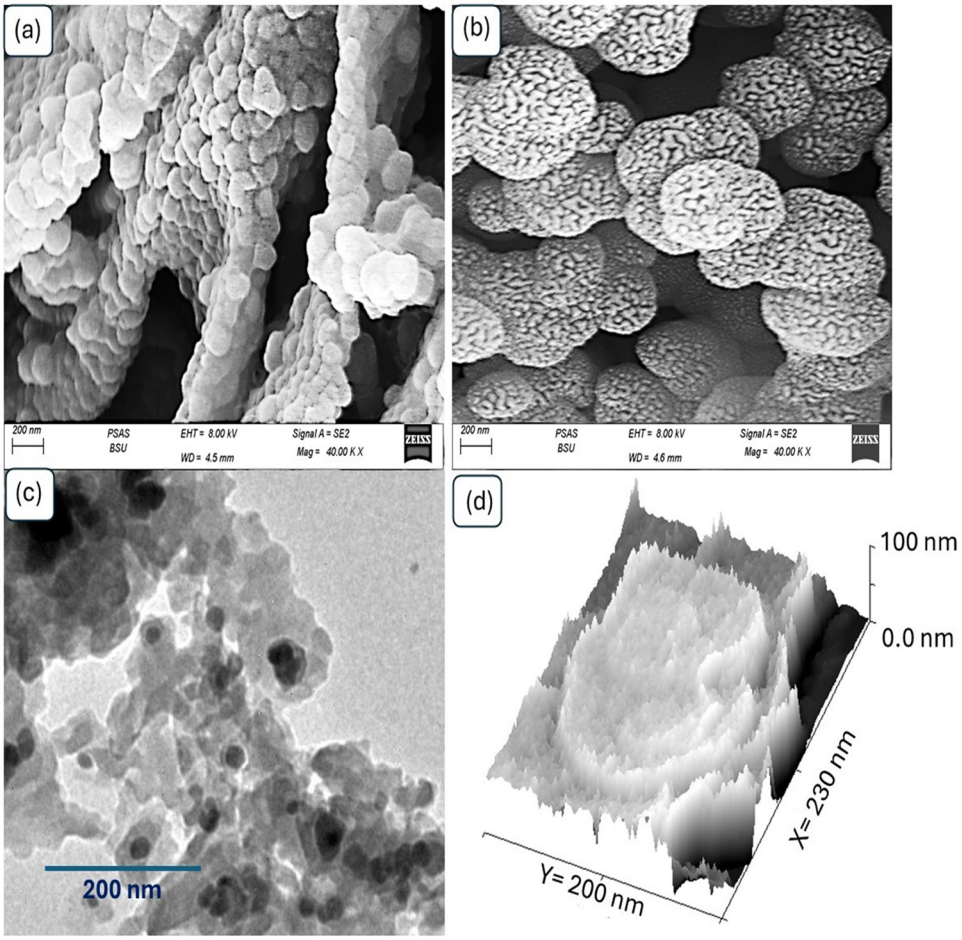

Figure 4: Morphological analyses of the Ag-Ag_2O-P1HP nanocomposite: (a) SEM, (c) TEM, and (d) theoretical modeling. (b) SEM of pristine P1HP.

analysis is approximately 80 nm. Additionally, a theoretical estimation of two contacting particles within the composite is conducted to evaluate the roughness and cross-sectional morphology. Each particle exhibits significant surface roughness, with an estimated diameter of 90 nm and a thickness of about 100 nm, reflecting the semi-spherical nature of the nanocomposite. Figure 4(b) illustrates the morphology of pristine P1HP, which has a spherical porous structure with a size of approximately 300 nm. This pristine polymer's features are crucial in understanding the composite's formation during the reaction with other materials. Overall, these analyses highlight the structural characteristics of the Ag-Ag_2O-P1HP nanocomposite. The SEM and TEM images show the well-ordered, semi-spherical nanoparticles and the embedded Ag-Ag_2O material within the P1HP matrix. The theoretical estimation provides further insight into the roughness and semi-spherical nature of the particles. The pristine P1HP's spherical porous structure also plays a significant role in the composite's formation. These morphological features collectively enhance the composite's potential for effective photon absorption and trapping, making it a promising material for various optical applications [30,31].

3.2 Green hydrogen using Ag-Ag_2O-P1HP/P1HP nanocomposite photocathode

The fabricated Ag-Ag_2O-P1HP nanocomposite, characterized by semi-spherical nanoparticles averaging 80–100 nm in size, exhibits significant morphological and optical properties. With a 1.8 eV small bandgap and strong optical absorption, this nanocomposite has been evaluated for its effectiveness in generating green hydrogen gas. The evaluation was conducted using a three-electrode cell, where the Ag-Ag_2O-P1HP/P1HP nanocomposite served as the primary working photocathode. The electrolyte used in this cell was sanitation water, which notably did not require any external sacrificial agents. This setup presents a promising approach for converting a harmful

electrolyte into a valuable source of renewable energy, ultimately producing green hydrogen. The presence of heavy metals in sanitation water acts as a driving force for ion movement, facilitating the reduction of water at the cathode to generate H_2 gas.

Under light illumination, the Ag-Ag_2O-P1HP/P1HP nanocomposite photocathode demonstrates excellent photocatalytic activity, as evidenced by the H_2 gas production shown in Figure 5(a). The variation in J_{ph} compared to the J_o is noted, with values of −0.22 and −0.14 mA/cm^2, correspondingly. This results in a photocurrent of 0.08 mA/cm^2, highlighting the photocatalytic efficiency of the photocathode. The effectiveness of this photocathode is attributed to its ability to generate a high electron density and an extensive electric field, which facilitate the production of hot electrons crucial for the photocatalytic reaction [32,33]. The inclusion of silver (Ag) as a plasmonic material enhances this process by generating surface plasmon resonance, thereby increasing the number of hot electrons that are directly transferred to the photocatalytic materials, where they drive the water-splitting reaction, resulting in the formation of hydroxyl (OH) radicals. These highly reactive OH radicals further attack other H_2O molecules, for the generation of H_2 gas. Figure 5(b) illustrates the behavior of the photocathode under chopped light conditions, where the alternating increase and decrease in current density indicate the photocathode's rapid and sensitive response to light. This response demonstrates the photocathode's ability to efficiently accept or lose electrons, crucial for sustaining the H_2 gas generation reaction. Additionally, the consistent cycles of current density changes reflect the high photocathode stability. The stability is attributed to the integration of inorganic materials, such as Ag and Ag_2O, within the polymer matrix of P1HP, which is further coated with the polymer. This coating provides the composite with enhanced anticorrosion properties, ensuring the longevity and reliability of the photocathode in the photocatalytic process. Overall, the Ag-Ag_2O-P1HP/P1HP nanocomposite exhibits excellent photocatalytic performance and stability, making it a promising material for green hydrogen production from sanitation water.

The impact of using individual monochromatic light sources to illuminate the Ag-Ag_2O-P1HP/P1HP nanocomposite photocathode is illustrated in Figure 6(a). The study utilized four different monochromatic wavelengths: 540, 440, 340, and 730 nm. The first three wavelengths – 540, 440, and 340 nm – demonstrated a significant effect on the photocathode, resulting in high J_{ph} of −0.19, −0.20, and −0.21 mA/cm^2, correspondingly. These high J_{ph} values indicate substantial hydrogen gas production. In contrast, the 730 nm wavelength achieved a lower J_{ph} value of −0.17 mA/cm^2, which is closer to the dark current density (J_o) values. As a result, the energy associated with this wavelength is insufficient to induce significant bond vibrations and therefore, only leads to limited H_2 gas production.

The difference in performance between the 730 nm wavelength and the other three wavelengths can be explained by the energy levels associated with these wavelengths. The photon energies for the 540, 440, and 340 nm wavelengths are 2.3, 2.8, and 3.6 eV, correspondingly, all of which exceed the estimated bandgap of the photocathode material, which is 1.8 eV. This means that these higher-energy wavelengths are capable of easily exciting electrons, promoting them to the conduction band. The presence of silver in the nanocomposite enhances this process by generating an electric field that

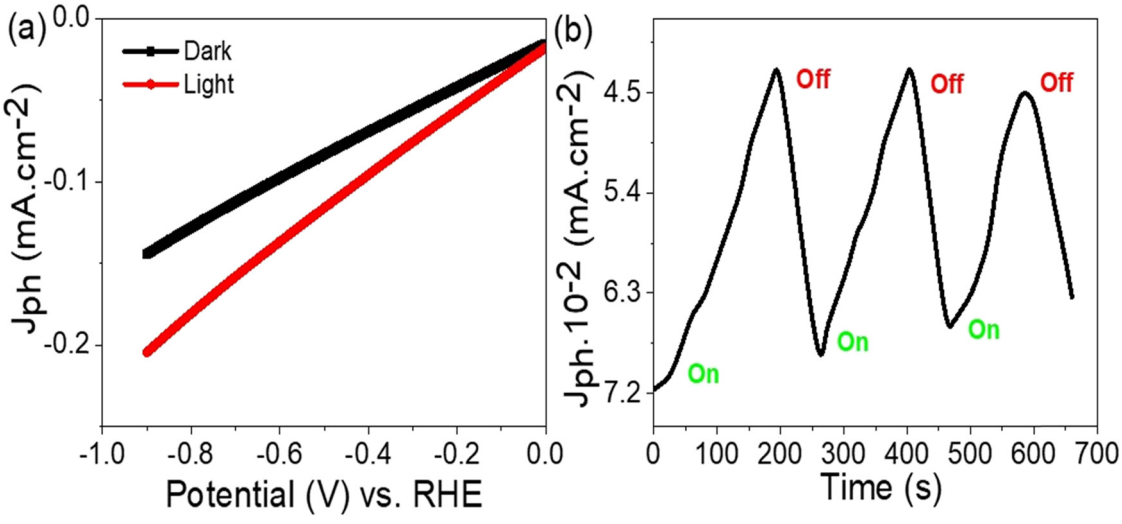

Figure 5: Green hydrogen production using the Ag-Ag_2O-P1HP/P1HP nanocomposite photocathode: (a) comparison of light and dark performance, and (b) response of chopped current under alternating light and dark conditions.

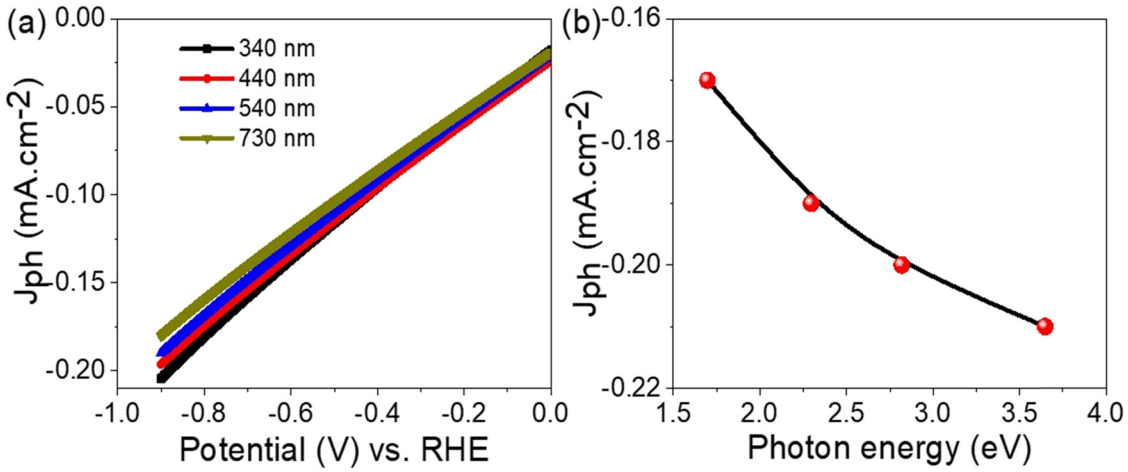

Figure 6: Green hydrogen production using the Ag-Ag_2O-P1HP/P1HP nanocomposite photocathode: (a) impact of different light wavelengths and (b) corresponding J_{ph} values at varying photon energies.

encompasses all the metal oxide and polymer components, thereby providing a large number of hot electrons that contribute to the high J_{ph} values and, consequently, to efficient H_2 gas generation [34].

Figure 6(b) further illustrates the relationship between the photon wavelength and the J_{ph} values, showing a clear trend of decreasing photocurrent density with increasing photon wavelength. This sequential decrease confirms that shorter wavelengths, which have higher photon energies, are more effective in driving the photocatalytic process and generating hydrogen gas compared to longer wavelengths like 730 nm, which fall below the energy threshold needed to effectively engage the photocathode material. This study underscores the importance of using light sources with photon energies that exceed the bandgap of the photocathode to maximize the efficiency of hydrogen production.

The significant photocurrent density achieved by the fabricated Ag-Ag_2O-P1HP/P1HP nanocomposite photocathode highlights the efficient charge transfer occurring within this composite, as depicted in Figure 7(a). In this system, Ag_2O and P1HP are the primary sources of electrons as estimated through the theoretical modeling roughness image. The electrons accumulate on the surface of Ag_2O, while the holes are collected on the surface of P1HP, moving in the opposite direction. Silver metal serves as the ultimate receptor for the hot electrons, which are then utilized to generate surface plasmon resonance [35–37]. This resonance creates a strong electric field that envelops all the materials in the composite.

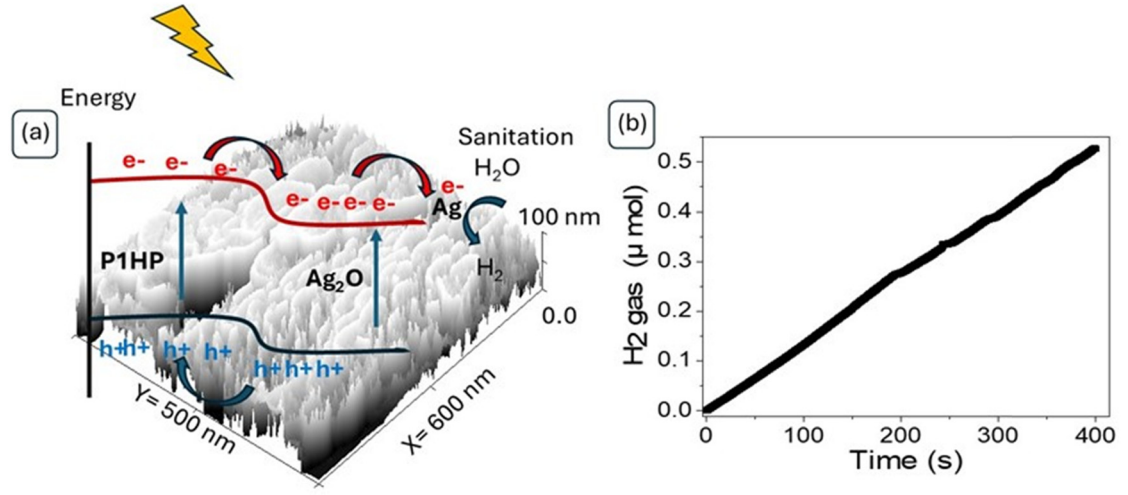

Figure 7: (a) Electron transfer within the fabricated Ag-Ag_2O-P1HP/P1HP nanocomposite photocathode and (b) the measured H_2 generation in moles using sanitation water.

Table 3: Comparison of the Ag-Ag_2O-P1HP/P1HP nanocomposite's performance with other studies on green H_2 gas generation

Photoelectrode	Electrolyte	J_{ph} (mA/cm^2)
Poly-3-methyl aniline/graphene oxide [38]	Sewage water	0.09
Polypyrrole/graphene oxide[39]	Sewage water	0.1
Polypyrrole/NiO [40]	Sewage water	0.11
Poly-O-aminothiophenol/intercalated iodide Composite [14]	Red Sea water	0.12
Cr_2S_3-Cr_2O_3/Poly-2-aminobenzene-1-thiol [22]	Sewage water	0.017
Ag-Ag_2O-P1HP/P1HP (this work)	Sewage water	0.22

The generation rate of 50 µmol/h per 10 cm² of this photocathode, as shown in Figure 7(b) and related to Eq. (1), further demonstrates the robust design of the Ag-Ag_2O-P1HP/P1HP nanocomposite. This photocathode is composed of various materials that exhibit high responsiveness to photon illumination and facilitate a sequential electron transfer process among its components. The result is the formation of a strong electric field on the surface, enhanced by the plasmonic properties of silver. This behavior also highlights the importance of sanitation water in hydrogen gas production, as the ions present facilitate significant mobility during the splitting reaction. This process leads to the formation of hydroxyl (OH) radicals, which serve as a driving force for water reduction *via* the fabricated photocathode.

These remarkable properties, combined with the efficient preparation methods and potential for large-scale production, make this photocathode highly promising. The superior performance of the Ag-Ag_2O-P1HP/P1HP nanocomposite is evident when compared to previous studies, as shown in Table 3. The data underscore the photocathode's advanced capabilities in generating green hydrogen, making it a strong renewable energy technology photocathode.

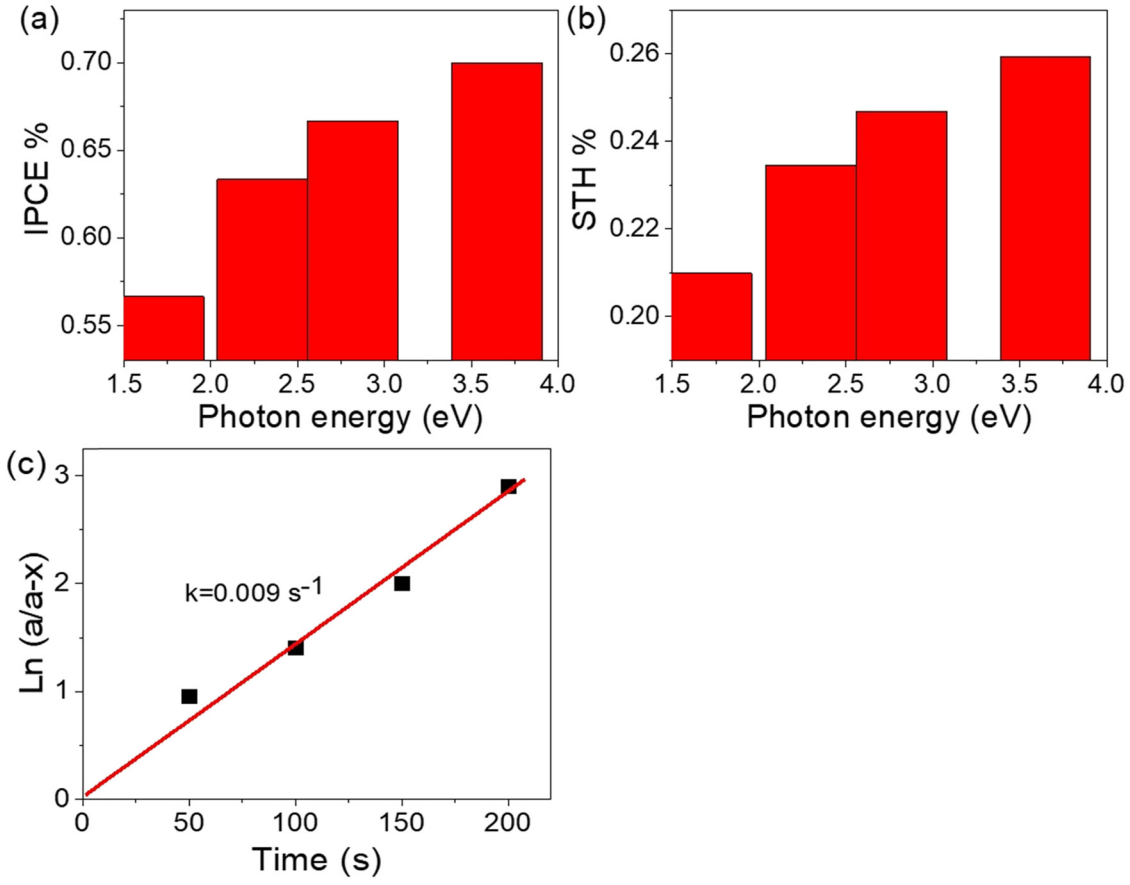

Figure 8: (a) IPCE and (b) STH efficiency for the fabricated Ag-Ag_2O-P1HP/P1HP nanocomposite reflects the green H_2 generation from sanitation water, and (c) the rate of the H_2 gas generation based on this photocathode.

The photon impact on the surface of the Ag-Ag_2O-P1HP/P1HP nanocomposite photocathode is assessed by calculating the IPCE using Eq. (2). The obtained values indicate the photocathode's strong performance in hydrogen generation, particularly in the UV region, where the IPCE reaches 0.7%. As the wavelength shifts toward the visible spectrum, the IPCE gradually decreases to 0.67% at 540 nm, followed by a further decline to 0.57% in the infrared region.

Similarly, the STH efficiency exhibits a comparable trend using Eq. (3). It peaks in the UV region with a maximum value of 0.26%, then diminishes to 0.23% in the visible range and continues to decrease to 0.21% in the infrared range. This pattern demonstrates that the photocathode's efficiency is highly dependent on photon energy, showing optimal performance under higher-energy photons.

The consistent decrease in both IPCE and STH efficiency from UV to IR regions highlights the photocathode's responsiveness to varying photon energies, confirming its suitability for hydrogen production. The results emphasize that the photocathode is most effective when exposed to higher-energy photons in the UV spectrum, while its efficiency gradually declines as the photon energy decreases in the visible and infrared regions. This behavior supports the potential application of the Ag-Ag_2O-P1HP/P1HP nanocomposite in photocatalytic processes, where its performance can be optimized by targeting specific regions of the electromagnetic spectrum.

Conversely, the rate constant (k) for hydrogen gas production using the fabricated photocathode is determined from Figure 7(c), with the calculated k value being 0.009 s^{-1} for a first-order reaction (Figure 8).

4 Conclusion

A new photocathode, Ag-Ag_2O-P1HP/P1HP, has demonstrated significant potential for green hydrogen production from sanitation water, achieving a rate of 50 µmol/h per 10 cm^2 using wastewater as the electrolyte in a three-electrode cell, without needing any external sacrificing agent. This nanocomposite features a bandgap of 1.8 eV, small crystalline material with a size of 32 nm, and semi-spherical nanoparticles ranging from 80 to 100 nm in diameter. The photocathode's performance was assessed by comparing its responsiveness in light, J_{ph}, and in the dark, J_o, with recorded values of −0.22 and −0.14 mA/cm^2, correspondingly.

The sensitivity of the photocathode was further tested with four monochromatic wavelengths: 540, 440, 340, and 730 nm. The first three wavelengths – 540, 440, and 340 nm – yielded high J_{ph} values of −0.19, −0.20, and −0.21 mA/cm^2, correspondingly, indicating substantial hydrogen generation. In contrast, the 730 nm wavelength produced a lower J_{ph} value of −0.17 mA/cm^2, as the energy at this wavelength is insufficient to trigger significant bond vibrations, resulting in reduced hydrogen production. The combination of high efficiency and the straightforward fabrication of this photocathode indicates its potential for scaling up as a prototype for industrial hydrogen generation applications. Additionally, the use of readily available and low-cost electrolytes addresses an environmental issue while also providing renewable energy sources.

Acknowledgments: Princess Nourah bint Abdulrahman University Researchers Supporting Project number (PNURSP2024R186), Princess Nourah bint Abdulrahman University, Riyadh, Saudi Arabia.

Funding information: Princess Nourah bint Abdulrahman University Researchers Supporting Project number (PNURSP2024R186), Princess Nourah bint Abdulrahman University, Riyadh, Saudi Arabia.

Author contributions: Mohamed Rabia: Experiments and writing. Maha Abdallah Alnuwaiser: Writing, funding, and supervision. All authors have accepted responsibility for the entire content of this manuscript and approved its submission.

Conflict of interest: The authors state no conflict of interest.

Data availability statement: All data generated or analyzed during this study are included in this published article.

References

[1] Kwon JH, Choi KC. Highly reliable and stretchable OLEDs based on facile patterning method: Toward stretchable organic optoelectronic devices. npj Flex Electron. 2024;8:17. doi: 10.1038/s41528-024-00303-5.

[2] Jovičević-Klug M, Souza Filho IR, Springer H, Adam C, Raabe D. Green steel from red mud through climate-neutral hydrogen plasma reduction. Nature. 2024;625(7996):703–9. doi: 10.1038/s41586-023-06901-z.

[3] Rabia M, Aldosari E, Zhang Q. Green hydrogen photoelectrochemically produced from Red Sea water using a photocathode dichalcogenides (CoS_2)-CoO/Poly-2-aminothiophenol nanocomposite with moon-like shape. Chem Pap. 2024;2024:1–13. doi: 10.1007/S11696-024-03478-3.

[4] El ouardi M, Idrissi AE, Ahsaine HA, BaQais A, Saadi M, Arab M. Current advances on nanostructured oxide photoelectrocatalysts for water splitting: A comprehensive review. Surf Interfaces. 2024;45:103850. doi: 10.1016/J.SURFIN.2024.103850.

[5] Zhang H, Zhang B, Wang X, Zou L, You J, Lin S. Effective charge separation in photoelectrochemical water splitting: A review from advanced evaluation methods to materials design. Sustain Energy Fuels. 2024;8:2357–82. doi: 10.1039/D4SE00390J.
[6] Kountouris I, Bramstoft R, Madsen T, Gea-Bermúdez J, Münster M, Keles D. A unified European hydrogen infrastructure planning to support the rapid scale-up of hydrogen production. Nat Commun. 2024;15:1–13. doi: 10.1038/s41467-024-49867-w.
[7] Giovanniello MA, Cybulsky AN, Schittekatte T, Mallapragada DS. The influence of additionality and time-matching requirements on the emissions from grid-connected hydrogen production. Nat Energy. 2024;2024:1–11. doi: 10.1038/s41560-023-01435-0.
[8] Constantinou P, Stock TJZ, Tseng L-T, Kazazis D, Muntwiler M, Vaz CAF, et al. EUV-induced hydrogen desorption as a step towards large-scale silicon quantum device patterning. Nat Commun. 2024;15:1–13. doi: 10.1038/s41467-024-44790-6.
[9] Li T, Wang B, Cao Y, Liu Z, Wang S, Zhang Q, et al. Energy-saving hydrogen production by seawater electrolysis coupling tip-enhanced electric field promoted electrocatalytic sulfion oxidation. Nat Commun. 2024;15:1–12. doi: 10.1038/s41467-024-49931-5.
[10] Purvis G, Šiller L, Crosskey A, Vincent J, Wills C, Sheriff J, et al. Generation of long-chain fatty acids by hydrogen-driven bicarbonate reduction in ancient alkaline hydrothermal vents. Commun Earth Environ. 2024;5:1–9. doi: 10.1038/s43247-023-01196-4.
[11] Ahmad I, Shukrullah S, Naz MY, Bhatti HN, Khalid NR, Ullah S. Rational design of ZnO–CuO–Au S-scheme heterojunctions for photocatalytic hydrogen production under visible light. Int J Hydrogen Energy. 2023;48:12683–98. doi: 10.1016/J.IJHYDENE.2022.11.289.
[12] Tsao CW, Narra S, Kao JC, Lin YC, Chen CY, Chin YC, et al. Dual-plasmonic Au@Cu_7S_4 Yolk@shell nanocrystals for photocatalytic hydrogen production across visible to near infrared spectral region. Nat Commun. 2024;15:1–13. doi: 10.1038/s41467-023-44664-3.
[13] Yan J, Hu L, Cui L, Shen Q, Liu X, Jia H, et al. Synthesis of disorder–order TaON homojunction for photocatalytic hydrogen generation under visible light. J Mater Sci. 2021;56:9791–806. doi: 10.1007/S10853-021-05896-0/FIGURES/12.
[14] Rabia M, Aldosari E, Geneidy AHA. Highly flexible poly-O-aminothiophenol/intercalated iodide composite with highly morphological properties for green hydrogen generation from Red Sea Water. Phys Scr. 2024;99:045001. doi: 10.1088/1402-4896/AD2BC5.
[15] Zang L, Liu Q, Qiu J, Yang C, Wei C, Liu C, et al. Design and fabrication of an all-solid-state polymer supercapacitor with highly mechanical flexibility based on polypyrrole hydrogel. ACS Appl Mater Interfaces. 2017;9:33941–7. doi: 10.1021/ACSAMI.7B10321/SUPPL_FILE/AM7B10321_SI_001.PDF.
[16] Trabelsi ABG, Elsayed AM, Alkallas FH, Rabia M. Flower-like Cr_2O_3-$Cr(OH)_3$/Poly-2-chloroaniline nanocomposite photoelectrode grown on polypyrrole film for hydrogen generation from sewage water. Opt Quant Electron. 2024;56:1–14. doi: 10.1007/S11082-023-05306-6/METRICS.
[17] Al Angari YM, Ewais HA, Rabia M. Hydrogen generation from Red Sea water using $CsSnI_2Cl$ lead-free perovskite/porous CuO nanomaterials: Coast of Jeddah, Saudi Arabia. J Mater Sci: Mater Electron. 2023;34:1–12. doi: 10.1007/S10854-023-11597-Y/METRICS.
[18] Shaban M, Rabia M, El-Sayed AMA, Ahmed A, Sayed S. Photocatalytic properties of PbS/graphene oxide/polyaniline electrode for hydrogen generation. Sci Rep. 2017;7:1–13. doi: 10.1038/s41598-017-14582-8.
[19] Rabia M, Mohamed HSH, Shaban M, Taha S. Preparation of polyaniline/PbS core-shell nano/microcomposite and its application for photocatalytic H2 electrogeneration from H_2O. Sci Rep. 2018;8:1107. doi: 10.1038/s41598-018-19326-w.
[20] Higashi T, Kaneko H, Minegishi T, Kobayashi H, Zhong M, Kuang Y, et al. Overall water splitting by photoelectrochemical cells consisting of $(ZnSe)_{0.85}(CuIn_{0.7}Ga_{0.3}Se_2)_{0.15}$ photocathodes and $BiVO_4$ photoanodes. Chem Commun. 2017;53:11674–7. doi: 10.1039/C7CC06637F.
[21] Hadia NMA, Abdelazeez AAA, Alzaid M, Shaban M, Mohamed SH, Hoex B, et al. Converting sewage water into H_2 fuel gas using Cu/CuO nanoporous photocatalytic electrodes. Materials. 2022;15:1489. doi: 10.3390/MA15041489.
[22] Rabia M, Elsayed AM, Alnuwaiser MA. Cr_2S_3-Cr_2O_3/Poly-2-aminobenzene-1-thiol as a highly photocatalytic material for green hydrogen generation from sewage water. Micromachines. 2023;14:1567. doi: 10.3390/MI14081567.
[23] Sayyah SM, Shaban M, Rabia M. A high-sensitivity potentiometric mercuric ion sensor based on m-toluidine films. IEEE Sens J. 2016;16:1541–8. doi: 10.1109/JSEN.2015.2505313.
[24] Padilla Villavicencio M, Escobedo Morales A, Ruiz Peralta MdeL, Sánchez-Cantú M, Rojas Blanco L, Chigo Anota E, et al. Ibuprofen photodegradation by Ag_2O and Ag/Ag_2O composites under simulated visible light irradiation. Catal Lett. 2020;150:2385–99. doi: 10.1007/S10562-020-03139-6/FIGURES/14.
[25] Lim DJ, Marks NA, Rowles MR. Universal Scherrer equation for graphene fragments. Carbon. 2020;162:475–80. doi: 10.1016/J.CARBON.2020.02.064.
[26] Burton AW, Ong K, Rea T, Chan IY. On the estimation of average crystallite size of zeolites from the Scherrer equation: A critical evaluation of its application to zeolites with one-dimensional pore systems. Microporous Mesoporous Mater. 2009;117:75–90. doi: 10.1016/J.MICROMESO.2008.06.010.
[27] Podder S, Pal AR. Plasmonic visible-NIR photodetector based on hot electrons extracted from nanostructured titanium nitride. J Appl Phys. 2019;126:083108. doi: 10.1063/1.5101009.
[28] Valenti M, Venugopal A, Tordera D, Jonsson MP, Biskos G, Schmidt-Ott A, et al. Hot carrier generation and extraction of plasmonic alloy nanoparticles. ACS Photonics. 2017;4:1146–52. doi: 10.1021/acsphotonics.6b01048.
[29] Zhan T, Ding G, Cao W, Li J, She X, Teng H. Amperometric sensing of catechol by using a nanocomposite prepared from Ag/Ag_2O nanoparticles and N,S-doped carbon quantum dots. Microchim Acta. 2019;186:1–9. doi: 10.1007/S00604-019-3848-0/FIGURES/7.
[30] AlAbdulaal TH, Ali HE, Ganesh V, Aboraia AM, Khairy Y, Hegazy HH, et al. Investigating $NaIO_3$ doped PVA polymeric nanocomposites via the structural morphology and linear and nonlinear optical analysis: For optoelectronic systems. Optik. 2021;245:167724. doi: 10.1016/J.IJLEO.2021.167724.
[31] AlAbdulaal TH, Yahia IS. Optical linearity and nonlinearity, structural morphology of TiO_2-doped PMMA/FTO polymeric nanocomposite films: Laser power attenuation. Optik. 2021;227:166036. doi: 10.1016/J.IJLEO.2020.166036.
[32] Konstantatos G, Badioli M, Gaudreau L, Osmond J, Bernechea M, Pelayo F, et al. Hybrid graphene-quantum dot phototransistors with ultrahigh gain. Nat Nanotechnol. 2012;7:363. doi: 10.1038/NNANO.2012.60.
[33] Ali AH, Ahmed AM, Abdelhamied MM, Abdel-Khaliek AA, Abd El Khalik S, Abass SM, et al. Synthesis of lead-free Cu/$CuFeO_2$/CZTS thin film as a novel photocatalytic hydrogen generator from

wastewater and solar cell applications. Opt Quant Electron. 2024;56(5):1–22. doi: 10.1007/S11082-024-06375-X.

[34] Sharma S, Kumar D, Khare N. Plasmonic Ag nanoparticles decorated Bi_2S_3 nanorods and nanoflowers: Their comparative assessment for photoelectrochemical water splitting. Int J Hydrogen Energy. 2019;44:3538–52. doi: 10.1016/j.ijhydene.2018.11.238.

[35] Zhang Y, Guo S, Xin X, Song Y, Yang L, Wang B, et al. Plasmonic MoO_2 as co-catalyst of MoS_2 for enhanced photocatalytic hydrogen evolution. Appl Surf Sci. 2020;504:144291. doi: 10.1016/J.APSUSC.2019.144291.

[36] Patel M, Pataniya PM, Sumesh CK. Enhanced photoresponse by plasmon resonance in Ni-WS_2/Si photodiode. Mater Res Bull. 2022;145:111518. doi: 10.1016/J.MATERRESBULL.2021.111518.

[37] Liang H, Sun H, Zhu Y, Fan L, Xu Q. Bi/Bi_2WO_6 plasmonic composites with enhanced photocatalytic activity for degradation of gasphase toluene. Catal Lett. 2023;153:559–69. doi: 10.1007/S10562-022-04001-7/METRICS.

[38] Helmy A, Rabia M, Shaban M, Ashraf AM, Ahmed S, Ahmed AM. Graphite/rolled graphene oxide/carbon nanotube photoelectrode for water splitting of exhaust car solution. Int J Energy Res. 2020;44:7687–97. doi: 10.1002/er.5501.

[39] Hamid MMA, Alruqi M, Elsayed AM, Atta MM, Hanafi HA, Rabia M. Testing the photo-electrocatalytic hydrogen production of polypyrrole quantum dot by combining with graphene oxide sheets on glass slide. J Mater Sci: Mater Electron. 2023;34:1–11. doi: 10.1007/S10854-023-10229-9/METRICS.

[40] Atta A, Negm H, Abdeltwab E, Rabia M, Abdelhamied MM. Facile fabrication of polypyrrole/NiOx core-shell nanocomposites for hydrogen production from wastewater. Polym Adv Technol. 2023;34:1633. doi: 10.1002/PAT.5997.